Available online at www.sciencedirect.com
SCIENCE DIRECT®
Microelectronic Engineering 82 (2005) 60–70
MICROELECTRONIC ENGINEERING
www.elsevier.com/locate/mee

Simulation of fluid flow in the step and flash imprint lithography process

Shravanthi Reddy, Roger T. Bonnecaze *

Department of Chemical Engineering and Texas Materials Institute, The University of Texas at Austin, 1 University Station CO400, Austin, TX 78712, United States

Received 9 February 2005; received in revised form 24 June 2005; accepted 30 June 2005
Available online 25 July 2005

Abstract

Step and flash imprint lithography (SFIL) is a photolithography process in which the photoresist is dispensed onto the wafer in its liquid monomer form and then imprinted and cured into a desired pattern instead of using traditional optical systems. The mask used in the SFIL process is a template of the desired features that is made using electron beam writing. Several variable sized drops of monomer are dispensed onto the wafer for imprinting. The base layer thickness at the end of the imprinting process is typically about 50 nm, with an approximate imprint area of one square inch. This disparate length scale allows simulation of the fluid movement between the template and wafer by solving governing equations of fluid mechanics simplified by lubrication theory. Capillary forces are also an important factor governing fluid movement; a dimensionless capillary number describes the relative importance of these forces to the viscous forces in the fluid. This paper presents a simulation to model the flow and coalescence of the multiple fluid drops and the effect the number of drops dispensed has on imprint time. The imprint time is shown to decrease with increasing numbers of drops or with an applied force on the template. Appropriate filling of features on the template is an important issue in SFIL, which is presented in this study by simulating the interface movement into and around the feature by a modified boundary condition on the governing equations. It is found that above a critical aspect ratio, features do not fill and fluid does not spread outside the mask edge. The simulation provides a predictive tool for understanding and optimizing fluid management in SFIL.

1. Introduction

The step and flash imprint lithography (SFIL) process offers a high-throughput, low-cost alternative to modern methods of lithography [1,2]. It avoids the use of costly optical systems for traditional projection printing and photolithography methods; instead, by using pattern transfer from masks made by electron beam writing, an image can be directly transferred to a substrate quickly and with much less expense than the electron beam writing of the mask itself. Electron beam

* Corresponding author. Tel.: +1 512 471 1497; fax: +1 512 471 7060.
E-mail address: rtb@che.utexas.edu (R.T. Bonnecaze).

0167-9317/$ - see front matter © 2005 Elsevier B.V. All rights reserved.
doi:10.1016/j.mee.2005.06.002

lithography produces a high quality image with nanometer scale features, but it is much too slow and expensive to be a viable method for chip manufacturing. Reproduction of this mask image by imprint lithography is, however, a potentially fast method using low cost tools that makes possible the manufacturing of high quality chips with nanometer scale features [3].

The SFIL process is illustrated in Fig. 1. It begins with dispense of an etch barrier in the form of a liquid monomer. The monomer may be dispensed, for example, using a piezoelectric pump that delivers several fluid droplets in a chosen pattern onto the substrate. Typically, the final resist layer is approximately 50 nm thick over a 1 in^2. imprint area. For an initial dispense of five equal size drops, the initial drop radii would be about 450 μm with a height of 20 μm at the center, assuming the monomer wets the wafer surface with a 5° contact angle. The monomer drops are pressed into the shape of the quartz mask by bringing the template down with a given speed or applied force; the chosen velocity or force may determine how well the monomer fills features in the template. The amount of time allowed for the actual imprinting as well as the force applied to the template will determine the base layer thickness of monomer on the substrate. Ideally, the drops merge and fill the template perfectly. The resulting mold is then "flashed" with UV light through the quartz template to photopolymerize the monomer. After the removal of the mask, the resulting polymer is etched through the base layer to produce the high aspect ratio features that make up the desired structure on the wafer surface. Features as small as 10 nm with 1:1 aspect ratios (before the etch) have been produced using this imprinting process [4]. Fig. 2 shows an example of such features.

While thermal imprint lithography (TIL), has also been successful in producing nanometer scale features [5–7], the procedure is much more time consuming and not as well suited for high-throughput, large-scale production of patterned wafers. In the TIL process, the wafer is coated with the polymer form of photoresist and the imprinting is performed above the polymer's glass-transition temperature. The pressures required for imprint are typically quite large in TIL, reportedly as high as 1900 psi [5], much higher than pressures used in SFIL; these high pressures can lead to

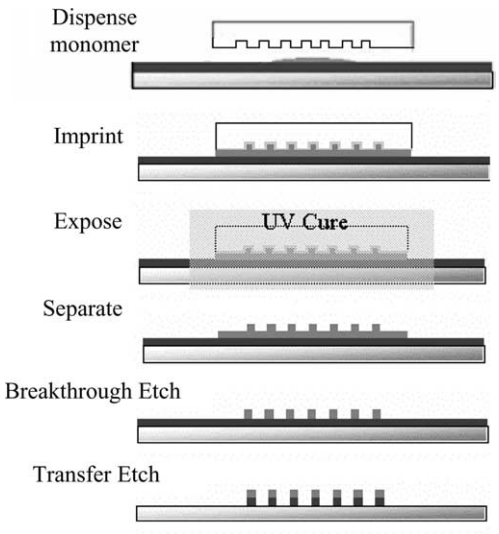

Fig. 1. Steps involved in the SFIL process. The treated mask (template) is pressed onto drops of liquid monomer. After UV cure and separation, etching produces high aspect ratio features.

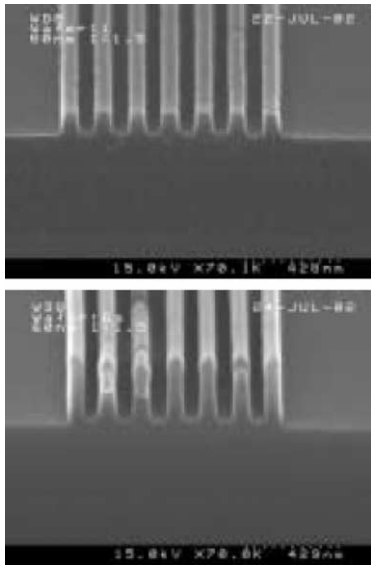

Fig. 2. SEM image of 60 nm lines after imprinting (top) and after etch processes (bottom), from Bailey et al. [3].

significant template deformation. The imprinting of a single layer of the highly viscous polymer form of the photoresist is not as effective as imprinting the liquid monomer, for which the lower viscosity fluid, use of multiple drops, and the advantage of capillary wetting allows for shorter imprint times [8].

Fluid dynamics is an important issue in the SFIL process. There is clearly a need for understanding the parameters that govern fluid flow of the liquid monomer between the substrate and the template. Issues that arise include the following: number of initial monomer drops and relative volume of drops dispensed, flow front arrest at edges of high aspect ratio features and template edges, air entrapment during feature filling, template velocity and force used for imprint, and imprint time.

In particular, this study explores the imprint time results for increasing numbers of monomer drops and for various patterns of drop dispense for a perfectly rigid template. A comparison is also made of the use of an applied force on the template to the case where there is a net zero force on the template. For the latter instance, the attractive capillary forces between the template and wafer are allowed to exactly balance the repellant viscous forces generated during the imprint process. As will be seen the, use of a net zero force on the template is advantageous if template distortion is a concern since it leads to a lower pressure variation across the template. The filling of features on the scale of the drops, such as large contact hole features, is also presented in this study. Fluid leakage out of the imprint area is another issue of concern that is discussed.

2. Simulation

As the plates approach each other, the curvature of the fluid–air interface exerts a capillary force that pulls the template to the wafer due to the surface tension of the monomer and its wetting nature on both surfaces, as shown in Fig. 3, where V represents the template velocity, R_0 is the initial drop radius, and h_0 is the initial gap height between the template and the wafer. Viscous forces

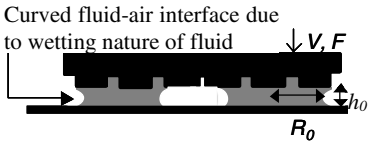

Fig. 3. Cross-section of template moving towards the substrate at velocity V or force F, pressing the monomer drops and causing them to spread through the channel.

exerted by the fluid balance this capillary force along with any applied force, F. The viscous forces arise from the fluid flow through the gap and the capillary forces arise due to the curved monomer–air interface that forms due to the wetting contact angles between the monomer and the plates.

Lubrication theory [9] allows simplification of the Navier–Stokes equations of motion for the case in which the gap height between the substrate and template is much smaller than the length scale of the drop. During the imprinting process, this is true due the relatively large size of the imprint area compared to the drop radii. Only at the end of the imprint process are the features significantly different in height compared to the base layer thickness; however, this irregularity is amended using a modified boundary condition, discussed shortly, and by the fact that volume conservation is rigorously ensured throughout the simulation. Thus, the following governing equations can be used to calculate the fluid's pressure and velocity field:

$$\nabla \cdot (H^3 \nabla P) = -12\mu V, \tag{1}$$

$$\mathbf{U} = \frac{-H^2}{12\mu} \nabla P, \tag{2}$$

where μ is the viscosity of the monomer, V is the downward velocity of the template, H is the gap height between the template and substrate at a given time in the process, P is the pressure in the fluid, and $\mathbf{U}$ is the vertically averaged, lateral velocity field. The boundary condition for solution of the lubrication equations accounts for the capillary force described. The pressure at the fluid–air interface, $P|_{\text{boundary}}$, depends upon the dominant radius of curvature of the interface, which can be written in terms of contact angles and the gap height

$$P|_{\text{boundary}} = P_{\text{atm}} - \gamma\left(\frac{\cos\theta_1 + \cos\theta_2}{H}\right), \tag{3}$$

where P_{atm} is the atmospheric pressure, γ is the surface tension, and θ_1 and θ_2 are the contact angles of the fluid with the template and the substrate, respectively. The contribution to the capillary pressure due to the other radius or curvature in the lateral direction or plan view of the template can be safely neglected since that pressure is $O(h_0/L)$ smaller than that in Eq. (3).

It is useful to non-dimensionalize the governing equations using characteristic values of the variables, namely $h_c = h_0$, $p_c = 12\mu VL^2/h_0^3$, and $u_c = VL/h_0$, so that $h = H/h_c$, $p = P/p_c$, and $u = U/u_c$. The lateral coordinates and ∇ operator are non-dimensionalized by L, the length of a side of the imprint area; h_0 is the initial gap height between the template and substrate. The resulting dimensionless equations and boundary conditions are given by

$$\nabla \cdot (h^3 \nabla p) = -1, \tag{4}$$

$$\mathbf{u} = -h^2 \nabla p, \tag{5}$$

$$p|_{\text{boundary}} = -\frac{1}{Ca}\frac{1}{h}, \tag{6}$$

where Ca is the dimensionless capillary number, which is given by

$$Ca = \frac{12\mu V}{\gamma(\cos\theta_1 + \cos\theta_2)}\left(\frac{L}{h_0}\right)^2. \tag{7}$$

The capillary number is the well-known ratio of the viscous force in the fluid to the capillary force caused by the surface tension of the fluid–air interface. A quantitative understanding of the interaction of these forces is important for controlling the movement of the template. For typical values of the parameters, such as $\mu = 1$ cP, $V = 1$ μm/s to 10 nm/s, $L = 2.54$ cm, $\gamma = 30$ dyn/cm, and $h_0 = 1$ μm, the capillary number can range from 10^{-2} to 1.

The primary weakness of lubrication theory is that it presents the governing equations for fluid flow in only two dimensions and is strictly only valid for slow variations of the height of the gap in the z-direction. Thus, rapid fluid movement in the vertical direction, i.e., into features on the template, cannot be explicitly tracked. In these cases the only way to predict fluid movement into a feature is to propose a mechanism for interface adjustment to fit into the feature. The discontinuous nature of such motion due to the sharp edges of the mask features, as shown in Fig. 4, must be accounted for using adjustments in the boundary condition.

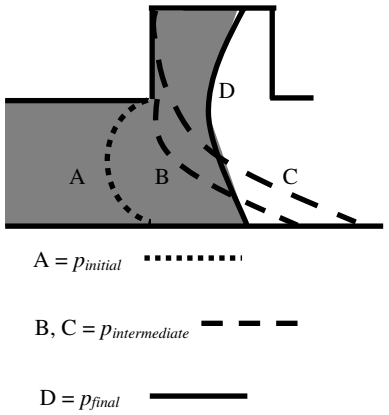

Fig. 4. Fluid–air interface goes through unstable, stretched conformations as it rounds the feature corner, until there is enough fluid for the interface to move into a stable conformation inside the feature.

Interface conformation "A" represents the interface just as it reaches the lower corner of a feature, where the boundary condition is a function of the gap height, h_{small}

$$p|_{\text{boundary}} = p_{\text{initial}} = -\frac{1}{Ca}\frac{1}{h_{\text{small}}}. \tag{8}$$

For example, if the capillary number is equal to one and the gap height has closed to 5% of the initial gap height ($h_{\text{small}} = 0.05$), this initial interface pressure, p_{initial}, is -20. The interface then effectively pins to the first corner of the feature (B), as the upper contact line negotiates around the feature corner while the bottom contact line moves along the wafer surface. The upper contact line then moves vertically to the top corner of the feature, at which point the stretched interface (C) is able to reconfigure into a stable low surface energy conformation (D) [10]. This interface advancement cannot be explicitly modeled by 2D lubrication equations alone, but it may be represented computationally at first as a pressure buildup at the interface, with a no flow restriction imposed at the boundary as follows:

$$\mathbf{n} \cdot \nabla p_{\text{intermediate}} = 0, \tag{9}$$

where $\mathbf{n}$ is the normal vector of the interface; solving this equation for $p_{\text{intermediate}}$ creates a pressure buildup for the boundary pressure at the interface. The interface finally moves into the feature and resumes a stable conformation of lower surface energy when this intermediate pressure exceeds the final pressure inside the feature

$$p_{\text{final}} = -\frac{1}{Ca}\frac{1}{h_{\text{large}}}, \tag{10}$$

where h_{large} is the height inside the feature. For a feature of aspect ratio 2 at the final gap height with h_{small} equal to 0.05, then h_{large} would be 0.1. Thus p_{final} is -10, a value greater than the interfacial pressure p_{initial}. Once the pressure buildup is achieved, the interface moves into the feature and fills the feature, and may be treated using the standard capillary boundary condition once again. There is no similar retardation of the interface for the case of flow from a large to small gap height, and so the standard pressure boundary condition is applied.

Using finite differencing methods to solve these equations numerically allows the calculation of the pressure and velocity fields in the fluid at a given time. The finite difference scheme is of second order accuracy; the typical grid size is 200×200 cells, for $\Delta x = 0.005$, to ensure less than 1% mass loss. Simulations with up to 400×400 cells were done and verified numerical convergence for the smaller number of cells. The volume of fluid (VOF) method [11] is used to move the fluid interface and thus track the fluid movement accurately. The method requires tracking the volumes of fluid in each cell in the numerical grid. Using velocity vectors on the faces of each cell, fluid volumes can be updated by summing the fluid entering the cell and subtracting the fluid leaving the cell at each time step. The time step size is determined by the maximum velocity vector in the domain to avoid fluxing an amount of fluid greater than the size of the cell

$$\Delta t = \alpha \frac{\Delta x}{V|_{\max}}, \tag{11}$$

where $V|_{\max}$ is the maximum velocity vector in the grid and α is a fraction (usually about 0.2) chosen to ensure conservation of total volume. By defining the fluid–air interface at a given volume fraction, e.g., cells that are half full, the fluid front can be tracked. Analytic expressions for the rate of a single drop spreading under a flat plate were used to check results from the simulation; strict volume conservation to within 1% is used to ensure valid results for all simulations. The process is assumed to occur in a vacuum or in a gas that is highly soluble in the monomer and so in the work discussed here, gas-trapping is neglected. The simulation is assumed to begin with fluid contacting both the substrate and template and immediate closure of the gap, so that evaporation of the monomer is neglected in the simulation.

3. Results and discussion

Many of the following studies are presented for a zero net force on the template, in the case where viscous forces and surface tension forces balance exactly. In this case the characteristic velocity V must be determined by balancing these two forces. The characteristic viscous force is related to the viscous pressure

$$F_{\text{V}} = p_{\text{c}} L^2 = \frac{12\mu V L^4}{h_0^3} \tag{12}$$

and the characteristic capillary force is related to the capillary pressure

$$F_{\text{C}} = \frac{\gamma(\cos\theta_1 + \cos\theta_2)}{h_0} L^2. \tag{13}$$

Equating these forces so they balance, the velocity of the template has a characteristic value

$$V = \frac{\gamma(\cos\theta_1 + \cos\theta_2)h_0^2}{12\mu L^2}. \tag{14}$$

Upon inserting this characteristic template velocity into the expression for the capillary number, the value $Ca = 1$ is obtained as our intuition might suggest, so that the following results are for simulations in which the template velocity is computed according to this force balance at a capillary number of one. Note also that the unity on the RHS of Eq. (4) is replaced at each time step by the dimensionless velocity that ensures a zero net force on the template.

3.1. Multiple drop simulation

Fig. 5 illustrates the use of the VOF method for merging multiple drops under a flat plate at zero net force and a capillary number equal to one. The pressure contours show that the drops behave much as one large drop immediately upon the merging of the interfaces, with the pressure field exhibiting a maximum in the center of the imprint area. It is also clear that pressure contours near the center have a circular shape as they would for a perfectly round drop, no matter what the shape of the coalesced drops. This is shown, for example, in the case of the final pressure field where the drops have taken the square shape of the imprint area but the interior pressure contour looks similar to the initial case for circular drops. It should also be noted that the pressures are smaller toward the end of the imprint process due to the very negative capillary pressures at the fluid–air interface.

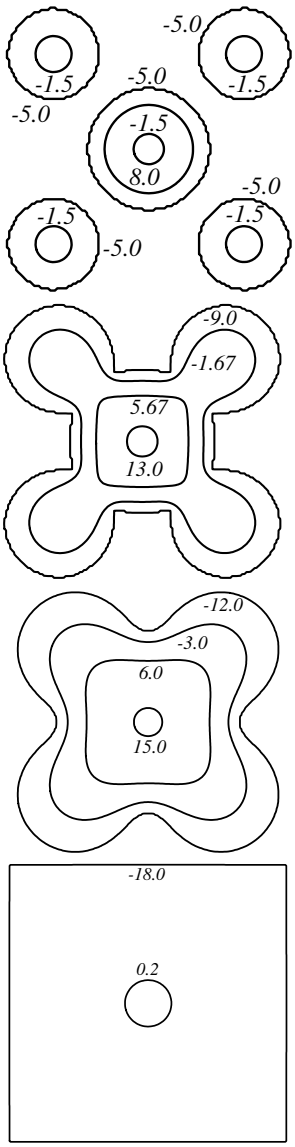

Fig. 5. Pressure contours for merging of five drops at $t = 0$, $t = 0.02$, $t = 0.06$, $t = 1.05$ and $Ca = 1$. The coalesced drops behave as a single drop with high interior pressure immediately after the drops merge. The lowest contour at each time step corresponds to the fluid-air interface.

The interface curvature in this plan view is negligible compared to the interface curvature in the profile view, due to the disparate length scales over which these planes exist. The length scale of the plan view is from $L/h_0 = 10^3$ to 10^6 times as large as the height of the gap in the profile view over the duration of the imprinting process. Thus, though there may be moments when the interface curvature is significant in the plan view, such as the initial moment two drops merge, these instances are extremely brief, so that the curvature in the plan view may safely be neglected.

This multiple drop simulation was used to study multi-drop spreading and merging under a flat plate to obtain the subsequent results in this section. The simulations were performed for a net zero applied force, so that the capillary forces exactly balance the viscous forces. The initial sizes of the drops were chosen so that their total volume would be equivalent to the final volume needed to fill a 50 nm gap between a flat template and wafer.

3.2. Imprint time

Simulations for increasing numbers of drops initially placed in a square array were performed for a template moving toward the wafer with zero applied force, the template velocity thus determined by balancing the capillary forces with the viscous forces. The results shown in Fig. 6 illustrate clear decrease of imprint time for increasing numbers of drops.

The curves move toward the single drop case when the drops merge and behave as a single drop;

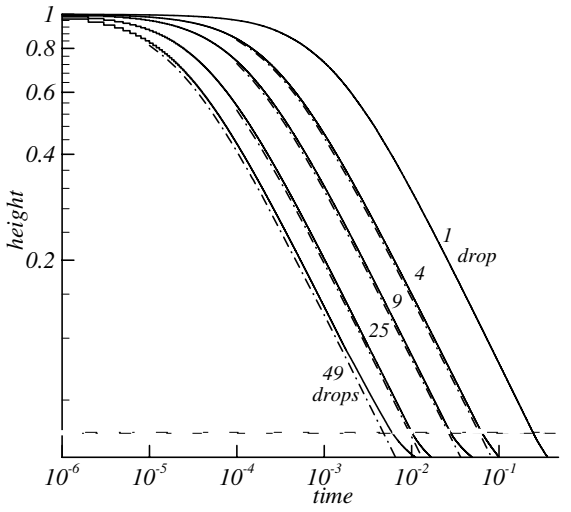

Fig. 6. Imprint time for increasing numbers of drops, with mask velocity determined by balance of capillary and viscous forces. Dotted curves represent approximate analytic solutions from scaling analysis. The horizontal dotted line represents the height at which the drops begin to merge.

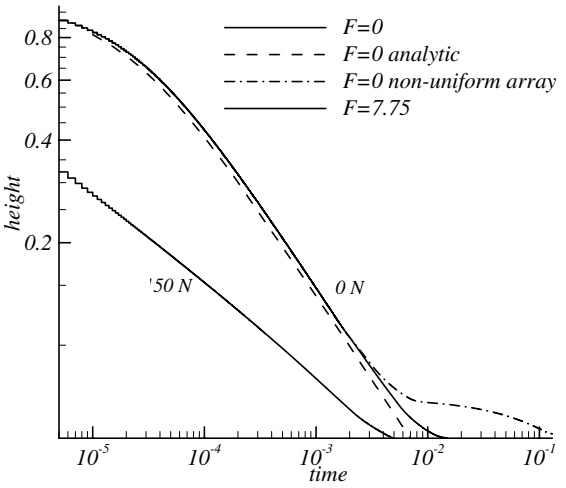

Fig. 7. Imprint time for 49 drops in a square array. A non-uniform distribution of the drops leads to longer imprint time, while applying a force of 50 N, corresponding to dimensionless value of 7.75, improves imprint time by a factor of 3.

this merge begins at the same gap height, $h_{\text{contact}} = 4h_f/\pi$, for any given number of drops with a total fixed volume, but the improvement in imprint time is still apparent. For a characteristic time of $t_c = 12\mu L^2/[h_0\gamma(\cos\theta_1 + \cos\theta_2)] = 129$ s, assuming $\theta_1 = \theta_2 = 0$, the imprint time for one drop is 65 s compared to an imprint time of 1.5 s for 49 drops. Fig. 7 illustrates the possibility of decreasing the imprint time by yet another order of magnitude by applying force to the template. The drawback in such a technique is that much higher pressures build in the fluid, on the order of 2.4 MPa as compared to only 450 kPa in the case of zero net force. This is an important consequence due to the issue of template deformation, which can occur if the pressures in the fluid are significant. While use of a net zero force alleviates high absolute pressures, it should be noted that large gradients in pressure could still exist, which can also contribute to template deformation. Deformations on the order of 70 nm for a 10 N force have been reported [12].

An approximate analytic solution is shown for each of the multiple drop cases, where the capillary forces balance with the viscous forces. This analytic approximation can be derived along the lines discussed by Colburn et al. [8] by solving Eq. (1) in its radial form for a single drop, namely

$$\frac{1}{r}\frac{\partial}{\partial r}\left(rH^3\frac{\partial P}{\partial r}\right) = -12\mu V. \tag{15}$$

With the boundary condition $P|_{r=R} = 0$, the pressure field is given by

$$P(r) = \frac{3\mu V}{H^3}(R^2 - r^2). \tag{16}$$

Integrating the pressure field over the area of the drop yields the viscous force F_V,

$$F_V = \frac{3\pi\mu V R^4}{2H^3}. \tag{17}$$

The applied force on the template is the sum of viscous and capillary forces on all the drops; neglecting the force applied by the contact line itself, which is negligible compared to the area of the drops, the applied force is given by

$$F_{\text{App}} = \left[\frac{3\pi\mu V R^4}{2H^3} - \gamma\left(\frac{\cos\theta_1 + \cos\theta_2}{H}\right)\pi R^2\right]N, \tag{18}$$

where N is the number of drops. Given the total volume of the N drops is $Q = \pi R^2 HN$, the velocity of the template is given by

$$V = -\frac{dH}{dt} = -\frac{2\pi}{3}\left[\frac{H^5 F_{App} N}{\mu Q^2} + \left(\frac{\hat{\gamma}}{\mu}\right)\frac{H^3 N}{Q}\right], \quad (19)$$

where $\hat{\gamma} = \gamma(\cos\theta_1 + \cos\theta_2)$.

Thus, there are two components that determine the template velocity; the first term on the right-hand side of Eq. (19) including F_{App} represents the applied force, whereas the second term on the right-hand side of Eq. (19) represents the capillary forces.

The dominant case may be determined by comparing the forces. The applied force dominates if

$$\frac{H^5 F_{App} N}{\mu Q^2} \gg \left(\frac{\hat{\gamma}}{\mu}\right)\frac{H^3 N}{Q} \quad (20)$$

or

$$\frac{H^2 F_{App}}{\hat{\gamma} Q} \gg 1 \quad (21)$$

and the capillary force dominates if the contrary is true. Thus, there exists two asymptotic behaviors for the template velocity; each expression for the velocity may be integrated to obtain the relationship between the gap height and time. For the case in which applied forces dominate

$$V = -\frac{dH}{dt} = -\frac{2\pi}{3}\left(\frac{H^5 F_{App} N}{\mu Q^2}\right) \quad (22)$$

or, nondimensionally

$$V = -\frac{dh}{dt} = -8\pi f_{App} N\left(\frac{h_0}{h_f}\right)^2 h^5, \quad (23)$$

where $f_{App} = F_{App} h_0/[\gamma(\cos\theta_1 + \cos\theta_2)L^2]$. This expression may be integrated to obtain the height as a function of time to give,

$$h = \left[1 + 32\pi f_{App} N\left(\frac{h_0}{h_f}\right)^2 t\right]^{1/4}. \quad (24)$$

This is the case in which a constant fixed force on the template causes the gap height versus time to decrease with a slope of $-1/4$ on the log–log plot shown in Fig. 7. Note that the analytical and numerical solutions for this case are indistinguishable.

For the case in which capillary forces balance the applied force, a similar integration of the velocity leads to

$$V = -\frac{dH}{dt} = -\frac{2\pi}{3}\left[\left(\frac{\hat{\gamma}}{\mu}\right)\frac{H^3 N}{Q}\right] \quad (25)$$

or, nondimensionally

$$V = -\frac{dh}{dt} = -8\pi N\left(\frac{h_0}{h_f}\right)h^3, \quad (26)$$

which may also be integrated to obtain an expression for the height as a function of time

$$h = \left[1 + 16\pi N\left(\frac{h_0}{h_f}\right)t\right]^{-1/2}, \quad (27)$$

where the gap height versus time decreases with a slope of $-1/2$, as shown for the dotted line analytic approximations in Fig. 6 and for the zero force cases in Fig. 7. These analytic approximations correspond extremely well to the simulation results, until the point where the drops merge and behave as one single drop, therefore moving away from the analytic approximation. If the drops are not placed in a uniform array in the imprint area, the drops merge before the final imprint thickness has been achieved, causing an order of magnitude increase in the imprint time and potentially high pressures in the fluid.

3.3. Feature fill

Varying aspect ratios of features will exist; these features will fill based on the boundary condition presented in the simulation section. The pressure jump that the interface must undergo will vary based on the current base layer thickness as it compares to the height of the feature. For a feature of aspect ratio 2:1, where the feature height is twice that of the final base layer thickness, the feature fills with some lag time as compared to the area around it, as depicted in Fig. 8(a). If the feature aspect ratio is increased slightly so that the feature is 2.5 times the thickness of the final base layer, i.e. 2.5:1 ratio, the feature does not fill, as shown in Fig. 8(b). This is because the pressure buildup behind the front of the fluid is insufficient to break into the large aspect ratio feature for this particular simulation. These results are for a single drop spreading under an otherwise flat plate, with zero net force on the template and a capillary number equal to one. The feature length and width were

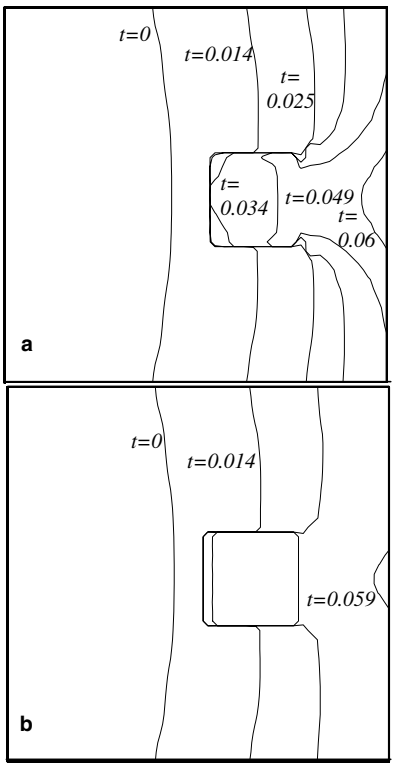

Fig. 8. Fluid interface snapshots during the imprint: (a) feature of aspect ratio 2:1 fills and (b) feature of aspect ratio 2.5:1 does not fill.

10% of the initial radius of the drop; results shown are for a very refined grid where $\Delta x = 0.0025$, but the filling results for the features were the same for a less refined grid where $\Delta x = 0.005$.

This technique can be used for any type of feature on the mask. Fig. 9 illustrates a line pattern filled by three drops with a dimensionless applied force of 7.75; the lines, which have a width equal to 10% the initial diameter of the drops and an aspect ratio of 2:1, do not fill immediately if the fluid interface must move into the high pressure region; however, the portion of the lines where the fluid drops are placed fill easily due to the drop flow along the line.

3.4. Feature density

In practice a template is composed of regions of high and low feature density, and the arrangement

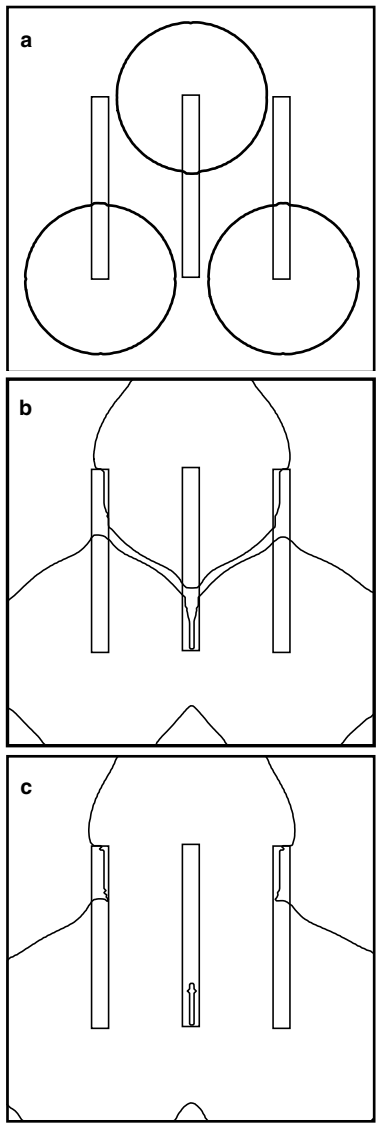

Fig. 9. Fluid interface snapshots during the imprint. The hole formed at the bottom of the center line in (c) is eventually filled by the end of the imprint process, assuming the surrounding medium is vacuum or highly soluble gas.

and size of droplets underneath can strongly affect the imprint time. In this case, areas on the mask with many features may be modeled as low volume areas, due to the presence of the features, as shown in Fig. 10. Imprint time can be improved in such a situation by placing drops of lower volume in the feature dense area of the mask, such that the total

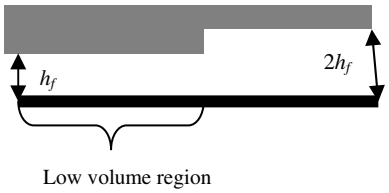

Fig. 10. Final gap height, h_f, in low volume area is half that in the high volume area, as for an area of the mask where features are very dense.

volume of the drops in the low volume region is half the volume of the drops in the high volume region. Imprint time results are shown in Fig. 11. It is apparent that the drop merge occurs closer to the end of the process for unequal sized drops, resulting in shorter imprint times. Using the characteristic time $t_c = 129$ s, the imprint time for 36 drops of unequal volume is an order of magnitude smaller, ~12 s, compared to the equal drop array or the four drop arrays, with imprint times of ~120 s.

3.5. Mask edge

For a single fluid drop spreading due to only the capillary action acting on a flat template (no applied force), the fluid does may or may not leak out of the mask edge. In general, the high aspect ratio of the mask edge confines fluid under the imprint area as seen in Fig. 1. Fluid travels preferentially along the mask edge for these high aspect ratio edges; however, fluid loss at the mask edge occurs for a lower aspect ratio edge, if the aspect ratio is less than 2:1 as shown in Fig. 12. The application of an applied force generally decreases the critical aspect ratio for fluid to leak out at the mask edge.

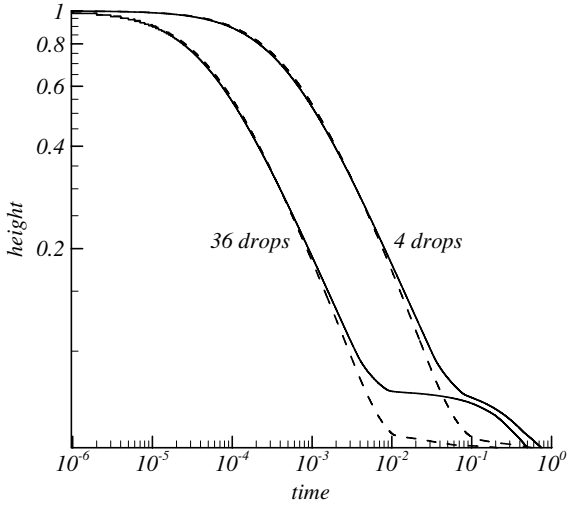

Fig. 11. Dashed lines represent unequal volume drops, where smaller drops are used in the low volume region. This adjusting drop volume improves imprint time.

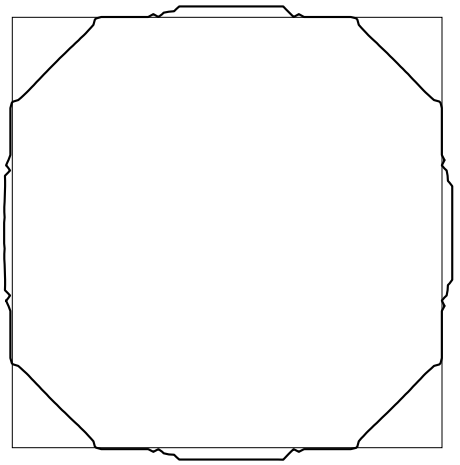

Fig. 12. For edges of aspect ratio 2:1, fluid leaks outside the imprint area before the final base layer thickness is achieved.

4. Conclusions

A dynamic, multi-drop simulation of fluid filling in step and flash imprint lithography has been presented. The foundation of the simulation is lubrication theory, which has been modified to handle flow into sharp features with a boundary condition that accounts for contact line dynamics at the corners of the features. The volume of fluid method is used to handle the merging of droplets and interfaces in the simulation.

Several fluid management issues critical to enhancing the speed and quality of the imprinting process were studied with the simulation. It has been shown that imprint time clearly decreases with the use of increasing number of droplets.

An applied force on the template may significantly reduce the imprint time compared to capillary action alone, though the higher fluid pressures encountered could lead to template deformation. It has also been shown that the density of features and their position on the mask may affect the imprint time, highlighting the necessity for varying the volume of the drops based on their position over the imprint area. Modeling of individual features and the mask edge has been presented with the use of a modified boundary condition, and it is clear that high aspect ratio features impede filling. This simulation thus provides a valuable tool for the analysis and optimal design of the SFIL fluid filling process.

Acknowledgments

This work was partially supported by DARPA Grant No. N66001-01-1-8964. SR also gratefully acknowledges the partial support of a College of Engineering Thrust Fellowship from The University of Texas and the guidance from P.R. Schunk and others in the Multiphase Transport Processes group at Sandia National Laboratories.

References

[1] T.C. Bailey, S.C. Johnson, S.V. Sreenivasan, J.G. Ekerdt, C.G. Willson, D.J. Resnick, J. Photopolymer Sci. Technol. 15 (3) (2002) 481–486.
[2] J. Haisma, M. Verheijen, K. Van den Heuvel, J. Van den Berg, J. Vac. Sci. Technol. B 14 (1996) 4124–4129.
[3] T.C. Bailey, S.C. Johnson, M.D. Dickey, B.J. Smith, A.T. Jamieson, E.K. Kim, N.A. Stacey, D. Mancini, W.J. Dauksher, K. Nordquist, D.J. Resnick, S.V. Sreenivasan, J.G. Ekerdt, C.G. Willson, in: Proceedings of the 39th Interface Symposium, 2002.
[4] M. Colburn, A. Grot, M. Amistoso, B.J. Choi, T. Bailey, J. Ekerdt, S.V. Sreenivasan, J. Hollenhorst, C.G. Willson, Proc. SPIE 3997 (2000) 435.
[5] S.Y. Chou, P.R. Krauss, P.J. Renstrom, J. Vac. Sci. Technol. B 14 (1996) 4129–4133.
[6] H.C. Scheer, H. Schulz, T. Hoffmann, S. Torres, J. Vac. Sci. Technol. B 16 (1998) 3917–3921.
[7] B. Heidari, I. Maximov, E. Sarwe, L. Montelius, J. Vac. Sci. Technol. B 17 (6) (1998) 2961–2964.
[8] M. Colburn, B.J. Choi, S.V. Sreenivasan, R.T. Bonnecaze, C.G. Willson, Microelectron. Eng. 75 (2004) 321–329.
[9] W.M. Deen, Analysis of Transport Phenomena, Oxford University Press, New York, 1998.
[10] S. Reddy, R.T. Bonnecaze, Phys. Fluids (submitted).
[11] C.W. Hirt, B.D. Nichols, J. Comp. Phys. 39 (1981) 201–225.
[12] S.D. Schuetter, G.A. Dicks, G.F. Nellis, R.L. Engelstad, E.G. Lovell, J. Vac. Sci. Technol. B. 22 (6) (2004) 3312–3317.